Nanomechanical characterization

Daniel Kiener* and Amit Misra*

Recent developments in test methodologies for nanoindenter-based small-length-scale mechanical characterization are overviewed, such as micropillar compression, cantilever beam bending, and tensile tests. Emphasis is placed on the possibilities offered by *in situ* testing in transmission and scanning electron microscopes, as well as examining strain rate and temperature dependence of mechanical strength. The versatility and growing impact of new nanomechanical characterization tools is highlighted through selected recent examples, such as indentation (sample) size effect, crack-tip plasticity, radiation damage, indentation creep, laser additive manufacturing, and crystalline/amorphous high-entropy alloys.

Introduction

In the 50-year history of the Materials Research Society (MRS), nanomechanical characterization is a relatively new field that has strongly emerged in the past three decades. In 1992, Oliver and Pharr published an analysis technique for instrumented, depth-sensing nanoindentation.[1] Their approach accounted for the curvature in the unloading data in determining the indentation depth, which together with the indenter tip calibration function can establish the contact area at peak load, thereby enabling accurate measurement of hardness and indentation elastic modulus of thin films without the need to optically image the indent to measure the area of impression. The Oliver–Pharr method[1] published in the *Journal of Materials Research*, a publication of MRS, currently has more than 29,000 citations according to Google Scholar, making it one of the most highly cited articles in the interdisciplinary materials research community. In fact, MRS meetings and their publications played a critical role in building and sustaining the nanomechanics research community that continues to grow and will be stronger and more vibrant in the next 50 years of MRS.

In this brief article, the authors have attempted to overview two aspects of nanomechanical characterization topical area of research. First, the developments in tools and test methods that have allowed the field to grow and attract a diverse group of researchers. The original nanoindentation hardness measurement following the Oliver–Pharr method is still used as a first-order characterization to extract hardness and modulus values of thin films on substrates and near-surface regions from shallow depth indents (typically, around 50–1000-nm deep). However, the characterization toolkit has been enhanced by developments such as focused ion beam (FIB), typically available as a dual-beam FIB/scanning electron microscope (SEM) instrument, for microfabrication of test geometries to enable compression, tension, and beam-bending tests from specific sites or features in the sample that the user can select in SEM/FIB. Today, the tests can be routinely conducted *in situ* in SEM or transmission electron microscopy (TEM) and can be performed over a range of temperatures and strain rates. Nanomechanical characterization is thus a complete laboratory for accelerated testing as well as in-depth exploration of specific deformation and fracture mechanisms under specified test parameters and environments. Second, we highlight a few selected examples, from the last 1–2 years, where recent developments in nanomechanical testing have provided new insights on classical problems such as indentation size effects, crack-tip plasticity, high-temperature creep, and radiation damage of metallic alloys, as well as relatively new material systems (crystalline/amorphous "high-entropy" alloys) and hierarchical nano-/microstructure alloys made by laser

Daniel Kiener, Department of Materials Science, Montanuniversität Leoben, Leoben, Austria; daniel.kiener@unileoben.ac.at
Amit Misra, Department of Materials Science & Engineering, and Department of Mechanical Engineering, University of Michigan, Ann Arbor, USA; amitmis@umich.edu
*Corresponding author

additive manufacturing (AM). Finally, we present a summary and future outlook in the field of nanomechanical characterization of metallic materials.

New tools and methods

Nanoindentation

Hardness testing as a widespread engineering technique for probing the strength of materials dates back to the early works of Mohs, Brinell, Martens, and others in the late 19th/early 20th century.[2] However, it was only with the development of modern highly automated depth-sensing nanoindentation devices and the related analysis routines enabling to determine very local elastic and plastic properties,[1] upon which nanohardness testing became the backbone of modern nanomechanical characterization in materials science. Concomitantly, the possibility to measure mechanical properties close to a material surface (**Figure** 1a) not only allowed to assess the characteristics of thin films,[3] but also resulted in the notion that the surface hardness of well-polished single crystals or individual grains increases with decreasing indentation depth,[4] a phenomenon referred to as the indentation size effect. Accounting for the dislocations necessary to realize the permanent imprint as geometrically necessary dislocations (GNDs), this size effect could be explained using strain gradient plasticity.[5] Furthermore, it turned out that nanoindentation data from defect-scarce materials volumes exhibited an elastic–plastic transition[6,7] referred to as pop-in, which allowed to assess the theoretical strength of materials and the related nucleation of dislocations[8,9] by adapting the contact theory of Hertz.[10] Implementation of lock-in amplifiers more recently further enhanced the technique, allowing for continuous determination of elastic and plastic properties, as well as the development of a number of advanced indentation protocols to comprehensively assess transient materials properties.[11] Facilitated by recent developments enabling experiments toward extreme conditions in terms of temperature, strain rate, or environment,[12,13] nanoindentation remains a backbone in modern material characterization of bulk materials[14,15] or thin films.[16,17] At the same time, emerging approaches such as high-throughput testing of small-scale structures[18,19] or machine learning-aided mapping of materials properties in complex structures[20,21] will affect the way nanoindentation devices are employed.

Focused ion beam microscopy

Another significant advancement in materials science was the introduction of focused ion beam (FIB) workstations.[22] The possibility to locally remove matter by scanning a FIB over the area to be removed would, for example, allow to perform a site-specific cross section for studying the material deformation taking place underneath a nanoindent,[23] or to extract a thin foil for TEM from the exact location of interest.[24] Moreover, using gas injection systems to introduce a precursor, it also became possible to deposit protecting layers or fix lifted materials to a micromanipulator to transfer and position them, which is still the state of the art for TEM and atom probe tomography sample preparation.[25] Despite all of its benefits, the FIB also offers some drawbacks, which mostly relate to the modification of the crystal structure by the impinging ion beam,[26] which have to be kept in mind in order to avoid for example unintended decoration of grain boundaries or liquid-metal embrittlement by Ga. In addition, the possible material volumes to be removed are limited to typical dimensions in the range of tens of microns. Therefore, recent developments are focusing on the one hand on using different ion species (e.g., He or Xe) for a more local or more massive material removal.[27] In the future, we could even see alloy ion sources that allow the scientist to switch between high sensitivity analysis using a light metal and large sputter yields by a heavy ion. On the other hand, developments toward using femtosecond pulsed laser ablation for massive material removal and structuring have been developed and commercialized,[28,29] allowing for large-scale material removal and 3D investigations in heterogeneous materials or for large representative volumes required, as well as enabling high-throughput sample fabrication.
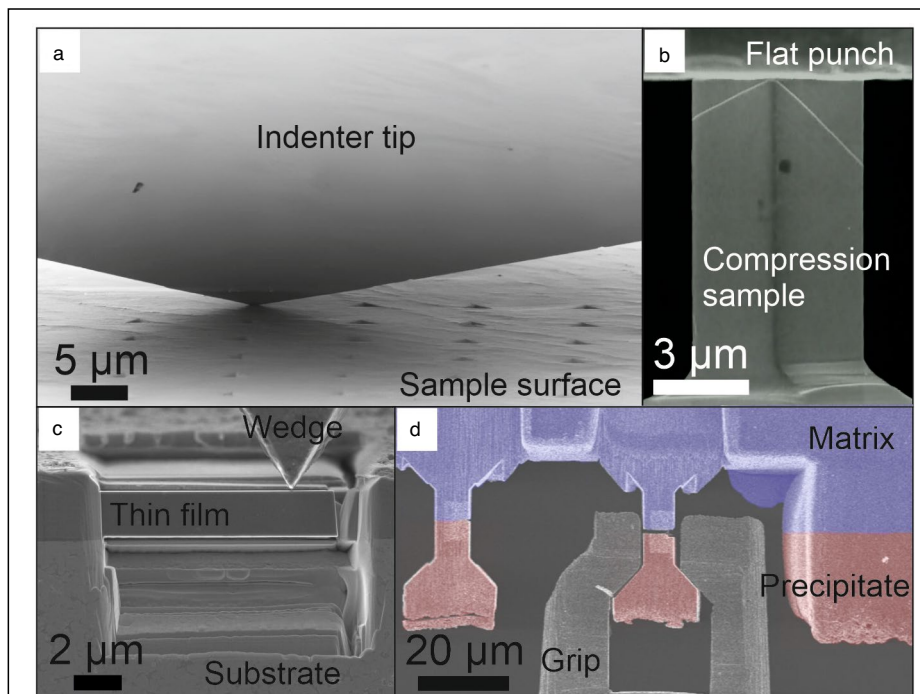

Figure 1. Examples of the most common miniaturized deformation experiments: (a) Nanoindentation, (b) microcompression testing, (c) beam bending, and (d) tensile testing.

Micropillar compression testing

Besides enabling scientists to take a look under the material surface or reconstruct 3D material volumes, the FIB also allowed them to locally remove material to shape miniaturized testing specimens, as pioneered by Uchic et al.[26] Loading these miniaturized compression specimens with a flat punch diamond tip in a nanoindentation device as shown in Figure 1b enabled one to probe the mechanical response of confined volumes in a site-specific nature, being it a nanocrystalline thin film, an ion implanted layer, a certainly oriented single crystal, or a specific grain boundary,[30] to name a few. This provided previously unseen freedom to micromechanical research that could otherwise only be addressed by much more demanding lithographic techniques[3] with all of their limitations in availability and flexibility. While the initial intention of the pioneering experiments was to remove the constraint of the multiaxial nanoindentation deformation geometry and probe the uniaxial response of confined volumes, the observation of sample size effect in single-crystal strength, in the absence of strain gradients that occur in sharp tip nanoindentation sparked the interest of many groups around the world and fused the field of micromechanics.[31] Concomitantly, this discovery promoted the experimental and simulation side to move closer together, as simulations could be conducted at comparable length scales for comprehensive miniaturized experiments.[32,33] Despite their many benefits, most notably the straightforward conversion from load–displacement to stress–strain data, these small-scale compression experiments also bear some shortcomings, such as potential taper and top rounding due to the ion-beam characteristics (e.g., type of ion, beam size and related beam tails), the additional compliance added by the base, including the fillet that requires attention to be corrected in the analysis, lateral deformation constraints, or the friction between platen and sample top.[34]

Cantilever bending experiments

Another geometry that was developed soon after the compression samples were bending beams, both rectangular[35] and triangular.[36] In the triangular beam, the entire film is subjected to a uniform state of plane strain as the beam is deflected, so it is useful in extracting stress–strain relation.[36] In the rectangular geometry, the bending is concentrated near the clamp end and with a sharp notch, it is useful in evaluating the crack-tip plasticity and fracture resistance.

From the experimental viewpoint, they are convenient to fabricate, and while square cross sections require exposure of the respective material cross section (Figure 1c), those with triangular or pentagonal geometry can be placed arbitrarily oriented on the sample surface. In addition, the loading is convenient, as conventional pointed tips can be employed, while wedge-shaped tips minimize potential torque. These benefits facilitated for example early works on studying elastic anisotropy[37] or strain gradient plasticity at (sub-) micron length scales,[35] or fracture testing of individual interfaces.[38] While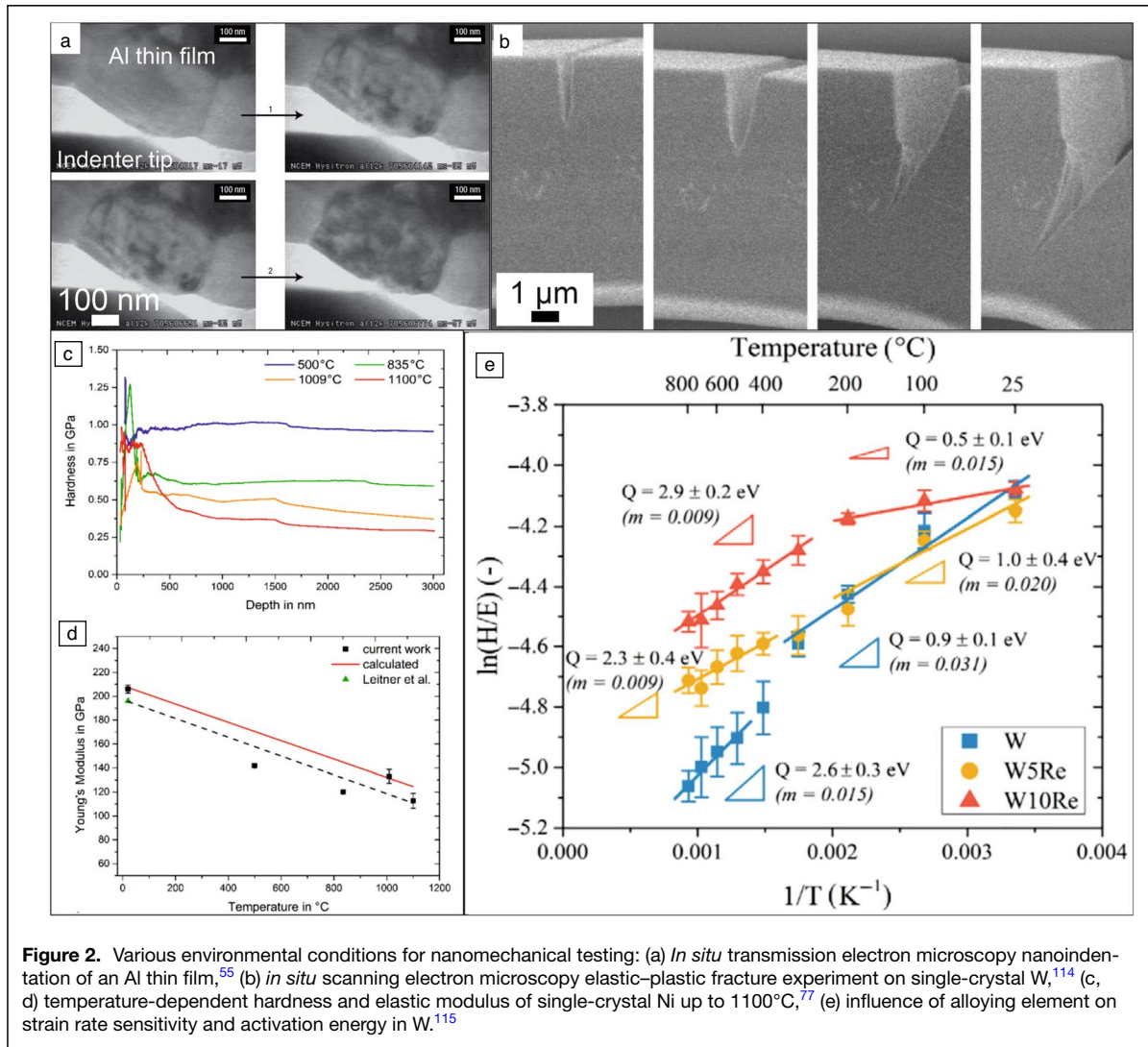 the inherent stress and strain gradient in these bending experiments can be of interest, its presence as well as additional compliances at the base of the beam commonly complicate the data analysis, and frequently an accompanying numerical finite element assessment is necessary to analyze the mechanical data.[39] Such bending experiments also offer convenient possibilities for full load reversal in cyclic deformation,[40] which is much more demanding to realize in a uniaxial fashion.[41] Finally, since the beams can be positioned exactly at or over a microstructural component of interest, and a FIB notch added at a precise position, to date, this geometry is most frequently used in miniaturized fracture examinations for the ease of application.[42,43]

Direct, supported, and push-to-pull tensile testing

As previously mentioned, miniaturized compression tests possess some inherent limitations. To overcome those and also provide access to properties such as the work-hardening or strain to failure of small volumes, tensile testing approaches were developed. These can be roughly grouped into three strategies, the direct pull,[44,45] supported pull,[46] or push-to-pull[47] approaches. The former uses again a FIB to fabricate a dog bone tensile sample, as well as a modified gripping tool to conduct the experiment (Figure 1d). While offering all the benefits of a freestanding tensile test in terms of minimized constraints, alignment issues, etc., setup of the experiment requires multiple axis alignment of sample and respective gripper, typically conducted in situ in an electron microscope. For the supported tensile testing, a dedicated microelectromechanical system (MEMS) is required, most commonly fabricated by lithography out of Si.[48,49] The specimen itself is either co-fabricated with the device,[50] or placed onto it by manipulation and fixation using ion-induced metal deposition or similar approaches.[51] While these MEMS designs are more intricate in their use and differ significantly with respect to their load application, data readout, etc., they typically limit alignment issues once the sample is fixed straight and rigid due to the guiding stiffer Si frame. Regarding push-to-pull approaches, here, a less complex etched Si-based frame transfers an applied compressive motion into a tensile load on the specimen, which spans across a gap between a fixed and a movable part. The sample positioning again requires a pick and place operation in the FIB, but actuation can be accomplished by a conventional nanoindenter pushing on the device, without the need for any highly precise alignment or in situ observation. For situations where additional loading or support frames are in place, one should keep in mind that they could also contribute to the overall load and stiffness measured, so breaking of the sample could be required to separate the contributions of specimen and frame.

In situ TEM nanomechanics

From the early days on, the curiosity to unveil what happens within a material when exposed to an external stimulus has motivated scientists to conduct experiments directly within electron microscopes, in particular the TEM with all its

Figure 2. Various environmental conditions for nanomechanical testing: (a) *In situ* transmission electron microscopy nanoindentation of an Al thin film,[55] (b) *in situ* scanning electron microscopy elastic–plastic fracture experiment on single-crystal W,[114] (c, d) temperature-dependent hardness and elastic modulus of single-crystal Ni up to 1100°C,[77] (e) influence of alloying element on strain rate sensitivity and activation energy in W.[115]

possibilities for structural and analytical investigations down to the atomistic details. Early mechanical experiments using deformation stages[52] would already allow detailed mechanistic observations. However, local stresses or strains could only be deduced from local features such as curved dislocations[53] or the local lattice strain.[54] With the advent of miniaturized nanoindentation devices or MEMS platforms, these loading features could also be integrated with TEM sample holders (**Figure** 2a), allowing to conduct fully quantitative nanoindentation experiments,[55] or even nanomechanical tests providing direct correlation between applied stress and ongoing deformation mechanisms.[56] In recent years, sparked by the developments of faster detectors enabling the mapping of diffraction information even during *in situ* deformation,[57] the determination of local crystallography and related strains became accessible with nanometer resolution,[58] providing previously unseen information on crystalline, semi-crystalline, or amorphous materials. While providing an incredible amount of otherwise inaccessible information on material mechanics on the nanoscale, the common concern regarding TEM experiments

resides in the presence of nearby free surfaces required for electron transparency. While this is less of a concern for studying nanomechanical objects, it can be for bulk materials, once for example, typical interaction distances between dislocations are truncated by the sample dimensions, as prominently highlighted by the "smaller is stronger" sample size effect.[31]

In situ *SEM nanomechanics*

Conducting mechanical experiments inside an SEM is an active field of research with a rich history of novel insights into the deformation and failure behavior of modern materials.[59,60] Furthermore, during deformation, the use of digital correlation can provide insightful local deformation information with respect to the global far-field loading.[61,62] Nanoindentation experiments can also be conducted *in situ* in the SEM to precisely position the diamond tip and monitor local deformation around the indent during imprinting.[63] However, it was really the mentioned smaller is stronger size effect that sparked the desire to observe what was happening during the deformation of such miniaturized single crystals

(Figure 1b) to explain this unexpected behavior.[44,64–66] Given the wide availability of SEM instruments and the adaptation of several commercial nanoindentation platforms for use in SEMs, this technique became widespread in recent years, with applications to almost any material and microstructure one can think of, spanning from single crystals or well defined bicrystals to nanocrystals, nanofoams, or nanolayers, to name a few, and loading modes ranging from quasistatic uniaxial loading to creep, cyclic loading and fracture (Figure 2b). Furthermore, in combination with local chemical information, electron channeling contrast imaging and electron backscatter diffraction (EBSD) analysis promotes the understanding of local phase formation and other crystallographic changes[60,67] taking place during deformation. With advances recently enabled by direct electron detectors, similar to the diffraction mapping in TEM, also in SEM we can expect a new reality of much faster[68] orientation analysis to manifest.

Variable temperature testing

Testing materials close to operating conditions in general[69] and addressing thermally activated materials properties in detail[70,71] have always been key interests in the field of materials science. Notably, for a broad range of temperature-dependent nanomechanical experiments, where frequently diamond as the best thermal conducting material out there is involved, it is indispensable to tackle the influence of thermal drift[72] and concomitantly account for possible interaction between the nanoindentation tip and the material examined.[73,74] Several high-temperature nanoindentation devices have been designed with different strategies to handle these issues,[75,76] which currently enable elevated temperature testing exceeding 1100°C[77] (Figure 2c). With such temperature control established, it was only a matter of using cryogenic cooling agents rather than water to lower the testing range of nanomechanics to the cryo regime.[78,79] The previously mentioned advances regarding *in situ* SEM nanomechancial testing capabilities, in particular the vacuum environment offered by the SEM, naturally suggest these setups for miniaturized testing at nonambient temperatures, as it limits oxidation issues and at the same time offers imaging capabilities to follow the deformation of micropillars[80] or track crack lengths during fracture experiments.[81] Notably, the much more accessible environment of an SEM chamber compared to the objective pole piece of a TEM promotes addition of cooling or thermocouples for improving system stability, which is why these developments are to date not available to the same level of maturity for *in situ* TEM experiments.

Material behavior at different strain rates

Similar to realistic operating temperatures, materials testing also requires examination at realistic strain rates,[14] which can be split into creep, quasistatic, and impact testing. Starting with nanoindentation approaches, during creep indentation using a load controlled instrument, a certain load is applied and held constant, while the change in displacement is recorded and commonly interpreted in terms of activation energy-based creep laws. One should, however, keep in mind that in this scenario an expanding plastic cavity is probed and the actual strain rate is ill determined.[82] In fact, for load controlled indentation testing using a Berkovich tip, a nominally constant ratio between loading rate and load, $\dot{P}/P$, translates to twice the indentation strain rate, $\dot{\varepsilon}_{ind}$, due to $P \sim h^2$.[71] In the creep segment $\dot{P}/P \cong 0$, and creep contributions from material and instrument need to be disentangled.[11] To overcome this, recent developments attempt to keep the pressure during the creep experiment constant to more closely mimic the macroscopic creep test.[83] In the quasistatic regime, testing materials at various constant strain rates allows to access properties such as strain rate sensitivity or activation volumes, which are important for many material systems, including bcc, hcp, or any form of nanostructured materials.[84] Here, abrupt strain rate changes during nanoindentation have significantly increased the data output as well as the site-specific nature of the information that can be acquired.[85] In conjunction with testing at variable temperatures (Figure 2d), this provides access to the activation energies of the underlying deformation processes (Figure 2e).[86] The field of high strain rate or impact testing was for a long period dominated by classical pendulum approaches,[87] and it was only rather recently that faster transducers allowed to measure data at controlled strain rates up to 10^3 s^{-1}.[88] Using newly designed nanoindentation transducers and even faster data readout in an impact configuration, even higher strain rates in the regime of 10^4 s^{-1} [89] are accessible today.

When probing miniaturized samples rather than running nanoindentation experiments, the issue of the rather undefined creep volume can be mitigated. However, a large number of specimens with an equivalent microstructure will in any case be necessary, and potential issues related to plastic instability and surface contributions need to be taken into account. Thus, unless a multitude of specimens can be fabricated (e.g., using lithography),[90,91] nanoindentation could be the more efficient way to move forward for these kinds of investigations.

Applications

In this section, a few examples are highlighted where nanomechanical characterization has provided new insights in critical scientific issues in small-scale mechanical behavior of structural materials. A comprehensive coverage of all the applications of the test methods listed in the "New tools and methods" section is outside the scope of this brief overview. The following examples are from recent work published in the last two years, where nanomechanical testing was used in conjunction with electron microscopy (SEM or TEM performed postmortem or *in situ*).

Indentation size effect

Recent work by Ma et al.[92] used precession electron-beam diffraction microscopy to characterize the dislocations under

nanoindents in single-crystal Ni for indent depths ranging from ≈100 to ≈3 μm. Deviation from the linear relationship in the H^2 versus $1/h$ plot predicted from the Nix–Gao model[5] was noted at indent depth below ≈400 nm. Such behavior can emerge from the fact that the dislocations are not confined to the initially envisioned hemispherical plastic zone.[93] Cross-sectional electron microscopy characterization showed that at relatively larger depths (≈800 nm), dislocation tangles and sub-boundaries were observed that would serve to confine dislocation glide to a small hemispherical plastic zone below the indenter contact, resulting in extra strain hardening from the GNDs in addition to the statistically stored dislocations, consistent with the physical mechanism underlying the Nix–Gao model. However, at shallower depths (100–200 nm), a diffuse (as opposed to self-organized) distribution of dislocations was observed, where individual dislocation lines could be resolved. It is postulated that akin to dislocation source limitation, mobile dislocations glide away from the indented zone (including escape to the free surface), leaving behind a relatively low dislocation density in the indented plastic zone, and could explain the deviation from linearity in the H^2–$1/h$ plot at shallow indentation depth.[93]

Crack-tip plasticity

Direct measurement of dislocation activity at crack tips is crucial in developing predictive models of toughness of semi-brittle materials (e.g., refractory metals), including refractory concentrated alloys. Recent work by Edwards et al.[91] utilized *in situ* SEM nanoindentation testing of notched microcantilever beams of tungsten of 3–5 μm height. Using a Pt-speckle pattern, digital image correlation (DIC) was employed to measure total strains and simultaneously, under loading, high-resolution EBSD was utilized to spatially map the elastic strains and calculate the distribution of GNDs, both at nanoscale resolution. The difference between the two provided a measure of the plastic strains at the crack tip. This study utilized the J-integral method to evaluate a conditional fracture toughness of 6.8 MPa m$^{1/2}$ for the 5-μm notched cantilever. Correlating the measured crack-tip stress fields with the plastic zones, it was shown that despite the significant dislocation tangles observed at the crack tip via postmortem TEM, the scarcity of mobile dislocation sources could explain the limited room-temperature toughness of refractory metals.

Crystalline/amorphous multilayers of "high-entropy" alloys

Nanoindentation, in conjunction with cross-section TEM characterization of the plastic zone, elucidated the deformation mechanisms in nanoscale thin-film multilayers, where the constituent layers are "high-entropy" alloys, namely nanotwinned FCC CrMnFeCoNi (Cantor alloy composition) and amorphous/nanoglass (Senkov alloy composition), respectively.[94] The high-entropy composite multilayers (HECMs) with 50-nm layers demonstrated simultaneously high hardness (5.6 GPa) and deformability due to the novel mechanism of the reorientation and agglomeration of granular nano-glasses in the TiZrNbHfTa layer, which enables more plastic activities compared with conventional uniform-density amorphous solids, in conjunction with the nanotwinned structure in the CrMnFeCoNi layer. Reducing layer thickness to 5 nm resulted in a maze-like amorphous structure and nanoscale granular amorphous structure in the CrMnFeCoNi and TiZrNbHfTa layers, respectively, with increased hardness to 7.8 GPa, however, at a loss of uniform plastic deformability. The HECM material systems present new opportunities for materials design exploiting synergy between size (nanolayer, nanotwin), structure (crystalline/nano-glass) and chemistry (multicomponent concentrated alloys) to develop strong and plastically deformable structural materials.

Laser additive manufacturing

Laser-based additive manufacturing (AM), via powder-bed fusion or directed energy deposition, has been widely adopted as the technology to directly 3D-print complex shape components from powders. While the current focus is to apply AM to commercially available alloys, laser processing also enables microstructure design far from equilibrium. Single laser track experiments are well suited for
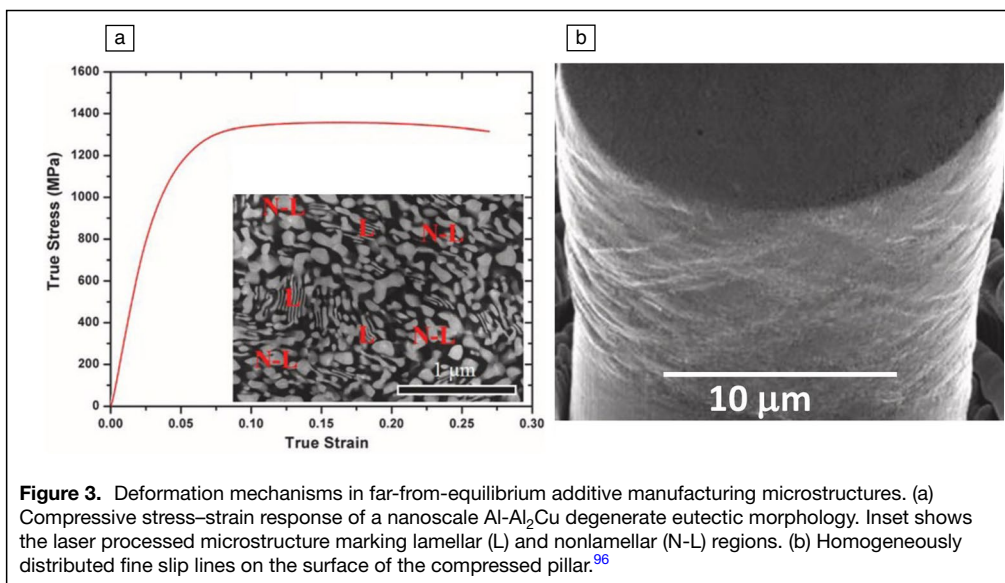

Figure 3. Deformation mechanisms in far-from-equilibrium additive manufacturing microstructures. (a) Compressive stress–strain response of a nanoscale Al-Al$_2$Cu degenerate eutectic morphology. Inset shows the laser processed microstructure marking lamellar (L) and nonlamellar (N-L) regions. (b) Homogeneously distributed fine slip lines on the surface of the compressed pillar.[96]
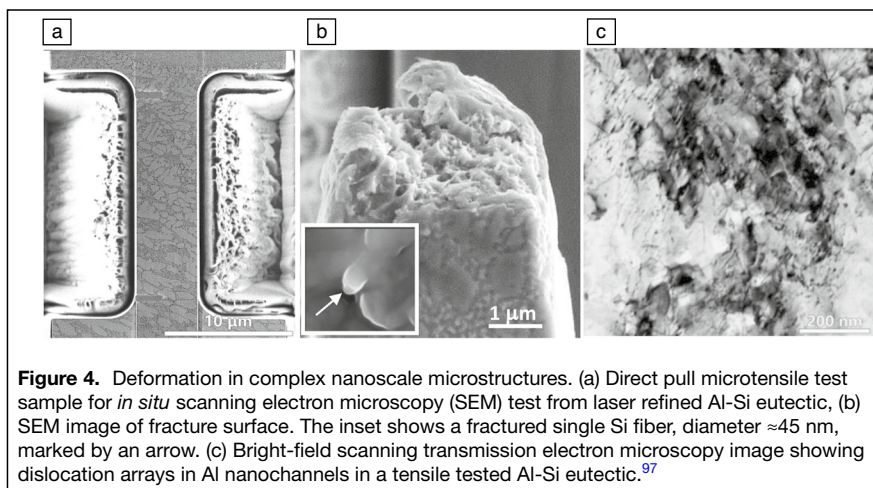
Figure 4. Deformation in complex nanoscale microstructures. (a) Direct pull microtensile test sample for *in situ* scanning electron microscopy (SEM) test from laser refined Al-Si eutectic, (b) SEM image of fracture surface. The inset shows a fractured single Si fiber, diameter ≈45 nm, marked by an arrow. (c) Bright-field scanning transmission electron microscopy image showing dislocation arrays in Al nanochannels in a tensile tested Al-Si eutectic.[97]

exploring the underlying processing–microstructure–property relationships through nanomechanical characterization of the melt pool.

As an example, laser remelting of Al-Al$_2$Cu eutectic produces nanolamellar microstructures, with interlamellar spacing refined to ≈20 nm, as well as degenerate nano-eutectic morphologies depending on the processing parameters.[95,96] Since the laser melt pool microstructure is polycrystalline with an eutectic colony of typically ≈1–5 μm, the diameter of the micropillar was varied from ≈4 to 15 μm, with the larger diameter used for polycrystalline average and the smallest diameter for testing a single colony with nano-lamellae oriented parallel, perpendicular, or inclined to loading axis. *In situ* pillar compression testing in the SEM is particularly useful in observing the shape change and deformation mode. For compression of single eutectic colonies, deformation mechanisms ranged from buckling and kinking in the parallel-loaded eutectics, planar sliding along Al–Al$_2$Cu lamellar interfaces in the incline-loaded eutectics (lowest strength) and localized shearing in the normal-loaded eutectics (highest strength), respectively. Highest compressive plasticity was observed in polycrystalline nanolamellar eutectics of ≈20-nm average spacing: >17% at flow stress of 1.63 GPa, and a degenerate, bimodal morphology (**Figure 3**): >11% at flow stress of 1.36 GPa (Figure 3a).[96] By comparison, the coarser eutectics failed at compressive strains of 2–3% reaching strengths of only ≈200 MPa. Overall, the key finding was that with decreasing interlamellar spacing, the strength increase was accompanied with slip lines uniformly distributed across the sample length (Figure 3b), as opposed to shear localization in coarser microstructures. Thus, the nanoscale heterogeneity (Figure 3a) of the structure actually promoted homogeneity of plastic flow at high flow strengths, exceeding 1 GPa in Al-based eutectic alloys.

Furthermore, direct pull *in situ* SEM tensile testing has been used to reveal the tensile strength-ductility synergy in laser rapid solidified Al-Si eutectic alloys, with tensile strengths approaching 600 MPa at uniform elongations exceeding 10 percent.[97]

SEM and STEM characterization shows that the microtensile samples can capture representative nanoscale microstructures (**Figure** 4a), and the tensile deformation and fracture behavior involved localized fracture of nano-Si fibers (Figure 4b) and finely spaced dislocation arrays in the Al nanochannels (Figure 4c). In conjunction with *in situ* tensile tests, cross-sectional STEM characterization of indents, using a Berkovich tip with 2 N load,[98] revealed the microstructure evolution in Al-Si eutectic with nanofibrous Si with increasing plastic strains. Underneath the indents, strain gradient plasticity is observed with the highest strain directly below the contact point and gradually decreasing to zero strain with increasing distance below the indent. Si nanofibers were observed to co-deform with the surrounding Al at low plastic strains, and exhibit shear cracks with increasing strains resulting in low aspect ratio fibers. In the region of the highest strains, Si "short" fibers (with an aspect ratio approaching unity) were located at the triple points of dynamically recovered nanograins in Al. These studies highlight that a combinatorial approach with *in situ* tension, compression, or indentation with postmortem S/TEM characterization of the plastic zone can provide quantitative assessment of the stress–strain response from site-specific samples and promote understanding of the involved dislocation mechanisms.

In addition to laser surface remelting of cast alloys, small-scale mechanical testing has also been used for characterization of laser direct energy deposited binary Fe–Cu alloys starting from elemental powders.[99] These alloys exhibit hierarchical microstructures with nanoscale precipitates of different sizes ranging from ≈4 to 25 nm and crystal structures arranged within micrometer-scale rapid solidified Fe and Cu grains. While Cu grains revealed metastable fcc Fe precipitates, the Fe grains contained both fcc Cu and finer, metastable bcc Cu precipitates. As compared to the strengths estimated from the Hall–Petch model of Fe and Cu grains of ≈1–2 μm, the compressive flow strength of the directed energy deposited microstructure was a factor of 3–4 higher, exceeding 900 MPa while maintaining plastic deformability to strains >30 percent.[99] In fact, site-specific small-scale mechanical testing using nanoindenter platforms has become a critical capability in research on additively manufactured multiphase alloys given the variations in the resultant melt pool microstructures.

Indentation creep in nanostructured alloys
In spite of the significant advances in the understanding of the mechanical behavior of nanoscale multilayered materials,[100] there are limited studies on high-temperature tensile and creep testing, due to limitations in tensile testing of bulk samples from nanostructured materials.[101] Recently, Zhang

et al.[102] demonstrated the use of nanoindentation in indentation creep studies up to 750°C in a commercial fcc MP35N alloy of nominal composition 34.1Ni–33.9Co–20.9Cr–10.2Mo–0.9Ti. Surface mechanical grinding treatment was used to refine grains, resulting in an average grain size of 42 ± 12 nm at ≈30-μm depth, where grain boundaries were interlocked with abundant twin boundaries, resulting in a thermally stable microstructure.

The mechanical tests involved loading within 5 s to the maximum load of 50 mN, and holding for 600 s to examine the creep response. Thermal drift was afterward estimated by dropping to 10% of the maximum load and holding for 600 s. With an indentation depth of 800 nm, the minimum reliable creep rate that could be obtained was ≈10^{-8}/s. The nanograined, nanotwinned single-phase microstructure was thermally stable, preserving its high strength at elevated temperatures, resulting in very low creep rates of ~10^{-7}/s at GPa-level stress at 700°C. These studies open new opportunities in exploration of the high-temperature creep behavior of thermally stable nanograined microstructures using nanoindentation creep testing.

Radiation damage

Academic research on structural metallic alloys for nuclear reactor applications is now routinely conducted using laboratory-scale ion irradiation as opposed to neutron radiation in a test reactor. Ion irradiation is fast and does not require handling radioactive materials after irradiation. However, it only produces near-surface damage, so nanoindentation-based methods are ideally suited for characterization of mechanical behavior after ion irradiation,[103–105] and could also be coupled with *in situ* TEM.[106–108] Since the mechanical strength also becomes dependent on the sample size at submicrometer length scales, it is critical to separate the effects of irradiation hardening from the indentation or smaller-is-stronger size effect. Based on *in situ* TEM compression tests on proton irradiated Cu nanopillars along the ⟨100⟩ direction with sample diameters ranging from 80 to 1500 nm, Kiener et al.[106] showed that size-independent yield strength was observed for diameters exceeding ≈400 nm, noticeably smaller as compared to approximately 2-μm dimensions observed for unirradiated Cu pillars.

The effects of grain and interphase boundaries that act as sinks for point defects[109] and alloy chemistries that offer improved irradiation and corrosion resistance such as the accident tolerant fuel cladding alloy FeCrAl[110] have received significant attention recently. Using *in situ* SEM micropillar compression testing, heterogeneous deformation responses along various crystallographic orientations were observed in FeCrAl alloys irradiated with 5 MeV Fe + ions at 300°C for doses ranging from 1 to 16 dpa on average.[111] Micropillars of ≈600-nm diameter and ≈1300-nm height were FIB machined from selected grains for single-crystal compression tests along low index directions, namely ⟨001⟩, ⟨110⟩, and ⟨111⟩. Based on postmortem TEM analysis of the irradiated and compressed pillars, it was shown that the irradiation-induced hardening results from the interaction between glide dislocations and radiation generated dislocation loops, and generally follows the prediction of the Orowan dispersed barrier hardening model. In all orientations, after approximately 3–5% strains, shear instability was observed. The flow stress corresponding to this is referred to as the "deformation instability stress." A direct linear scaling was noted between the deformation instability stress and the 0.5% offset yield stress for all three crystal orientations and irradiation doses up to 16 dpa. Cross-sectional postmortem TEM of the deformed pillars showed that the localized shear instability is caused by avalanche slip events of ½ ⟨111⟩ dislocations gliding out of compressed pillars.

Summary and future outlook

Given the broad range of small-scale tests that can be performed today with a nanoindenter test platform, such as depth-sensing indentation, pillar compression, direct pull tension, cantilever beam bending, etc., well controlled over a range of temperatures and strain rates, there has been widespread application of small-scale testing in materials research. The field of nanomechanical characterization significantly benefited from new tools such as FIB for microfabrication of desired test geometries from specific sites in the material, and *in situ* test platforms in SEM and TEM, respectively. In some communities such as structural materials for nuclear energy, small-scale testing has made a transformative impact in accelerating the materials testing and development by using ion irradiation in conjunction with nanomechanics. The fundamental study of sample size (volume) effects on the measured mechanical strength saw a renaissance driven by the development of new FIB and nanomechanical characterization tools. For a large number of nanostructured, nanocomposite and nano-laminate materials, new deformation mechanisms at "nano" length scales could be discovered using a combination of FIB-fabricated samples, nanomechanical testing and *in situ* or *post mortem* electron microscopy. Finally, the small-scale and local microstructure effects and accelerated testing of otherwise bulk materials such as "high-entropy" alloys, laser additive manufactured metallic alloys and metallic glasses have also been made possible via novel tools in nanomechanical characterization.

In short, the revolution that started with the nanoindentation testing for hardness and elastic modulus measurement of thin films has expanded broadly to cover bulk and new material classes, a range of tests and *in situ* observations covering not just elastic/plastic deformation but also fracture, creep, and irradiation damage. There are many other application areas, such as tribology, fatigue, stress corrosion cracking, hydrogen embrittlement, high strain rate nanoindentation, etc., where nanomechanical characterization has made an impact. While these topics could not be discussed here, given the significance of these fields, there have been other recent reviews that the reader is referred to for a more comprehensive

understanding of the current state of the art in nanomechanical characterization.[19,43,87,112,113]

Author contributions

Funding

Data availability

Data will be provided by the authors upon reasonable request.

Conflict of interest

On behalf of all authors, the corresponding author states that there is no conflict of interest.

Open Access

References

1. W.C. Oliver, G.M. Pharr, *J. Mater. Res.* **7**(6), 1564 (1992)
2. S.M. Walley, *Mater. Sci. Technol.* **28**(9–10), 1028 (2013)
3. W.D. Nix, *Metall. Mater. Trans. A* **20**(11), 2217 (1989)
4. W.J. Poole, M.F. Ashby, N.A. Fleck, *Scr. Mater.* **34**(4), 559 (1996)
5. W.D. Nix, H. Gao, *J. Mech. Phys. Solids* **46**(3), 411 (1998)
6. W.W. Gerberich, S.K. Venkataraman, H. Huang, S.E. Harvey, D.L. Kohlstedt, *Acta Metall. Mater.* **43**(4), 1569 (1995)
7. T.F. Page, W.C. Oliver, C.J. McHargue, *J. Mater. Res.* **7**(2), 450 (1992)
8. Y. Gaillard, C. Tromas, J. Woirgard, *Philos. Mag. Lett.* **83**(9), 553 (2003)
9. A. Gouldstone, K.J. Van Vliet, S. Suresh, *Nature* **411**(6838), 656 (2001)
10. K. Durst, B. Backes, O. Franke, M. Göken, *Acta Mater.* **54**(9), 2547 (2006)
11. K. Durst, V. Maier, *Curr. Opin. Solid State Mater. Sci.* **19**(6), 340 (2015)
12. D. Kiener, M. Wurmshuber, M. Alfreider, G.J.K. Schaffar, V. Maier-Kiener, *Curr. Opin. Solid State Mater. Sci.* **27**(6), 101108 (2023)
13. A. Barnoush, P. Hosemann, J. Molina-Aldareguia, J.M. Wheeler, *MRS Bull.* **44**(06), 471 (2019)
14. C.A. Schuh, *Mater. Today* **9**(5), 32 (2006)
15. A. Gouldstone, N. Chollacoop, M. Dao, J. Li, A.M. Minor, Y.L. Shen, *Acta Mater.* **55**(12), 4015 (2007)
16. G.H. Balbus, M.P. Echlin, C.M. Grigorian, T.J. Rupert, T.M. Pollock, D.S. Gianola, *Acta Mater.* **156**, 183 (2018)
17. W.D. Nix, *Mater. Sci. Eng. A* **234–236**, 37 (1997)
18. A. Jelinek, S. Zak, M. Alfreider, D. Kiener, *Adv. Eng. Mater.* **25**(7), 2200288 (2023)
19. D.S. Gianola, N.M. Della Ventura, G.H. Balbus, P. Ziemke, M.P. Echlin, M.R. Begley, *Curr. Opin. Solid State Mater. Sci.* **27**(4), 101090 (2023)
20. S. Vranjes-Wessely, D. Misch, D. Kiener, M.J. Cordill, N. Frese, A. Beyer, B. Horsfield, C. Wang, R.F. Sachsenhofer, *Int. J. Coal Geol.* **247**, 103847 (2021)
21. J.M. Wheeler, B. Gan, R. Spolenak, *Small Methods* **6**(2), e2101084 (2022)
22. M.W. Phaneuf, *Micron* **30**(3), 277 (1999)
23. D. Kiener, R. Pippan, C. Motz, H.G.M. Kreuzer, *Acta Mater.* **54**(10), 2801 (2006)
24. L.A. Giannuzzi, F.A. Stevie, *Micron* **30**(3), 197 (1999)
25. M.K. Miller, K.F. Russell, K. Thompson, R. Alvis, D.J. Larson, *Microsc. Microanal.* **13**(6), 428 (2007)
26. C.A. Volkert, A.M. Minor, *MRS Bull.* **32**(5), 389 (2007)
27. K. Höflich, *Roadmap for Focused Ion Beam Technologies* (Ferdinand Braun Institut, Berlin, 2023)
28. M.J. Pfeifenberger, M. Mangang, S. Wurster, J. Reiser, A. Hohenwarter, W. Pfleging, D. Kiener, R. Pippan, *Mater. Des.* **121**, 109 (2017)
29. M.P. Echlin, M. Straw, S. Randolph, J. Filevich, T.M. Pollock, *Mater. Charact.* **100**, 1 (2015)
30. J.R. Greer, J.T.M. De Hosson, *Prog. Mater Sci.* **56**(6), 654 (2011)
31. M.D. Uchic, D.M. Dimiduk, J.N. Florando, W.D. Nix, *Science* **305**(5686), 986 (2004)
32. J.A. El-Awady, *Nat. Commun.* **6**, 5926 (2015)
33. T. Zhu, J. Li, *Prog. Mater Sci.* **55**(7), 710 (2010)
34. D. Kiener, C. Motz, G. Dehm, *Mater. Sci. Eng. A* **505**(1–2), 79 (2009)
35. C. Motz, T. Schöberl, R. Pippan, *Acta Mater.* **53**(15), 4269 (2005)
36. J.N. Florando, W.D. Nix, *J. Mech. Phys. Solids* **53**(3), 619 (2005)
37. D.E.J. Armstrong, A.J. Wilkinson, S.G. Roberts, *J. Mater. Res.* **24**(11), 3268 (2009)
38. D.E.J. Armstrong, A.J. Wilkinson, S.G. Roberts, *Philos. Mag. Lett.* **91**(6), 394 (2011)
39. J. Gong, A.J. Wilkinson, *Philos. Mag.* **91**(7), 1137 (2011)
40. D. Kiener, C. Motz, W. Grosinger, D. Weygand, R. Pippan, *Scr. Mater.* **63**(5), 500 (2010)
41. S. Lavenstein, J.A. El-Awady, *Curr. Opin. Solid State Mater. Sci.* **23**(5), 100765 (2019)
42. R. Pippan, S. Wurster, D. Kiener, *Mater. Des.* **159**, 252 (2018)
43. B.N. Jaya, *MRS Bull.* **47**(8), 832 (2022)
44. D. Kiener, W. Grosinger, G. Dehm, R. Pippan, *Acta Mater.* **56**(3), 580 (2008)
45. G. Richter, K. Hillerich, D.S. Gianola, R. Mönig, O. Kraft, C.A. Volkert, *Nano Lett.* **9**(8), 3048 (2009)
46. D.S. Gianola, C. Eberl, *J. Mater.* **61**(3), 24 (2009)
47. H. Guo, K. Chen, Y. Oh, K. Wang, C. Dejoie, S.A. Syed Asif, O.L. Warren, Z.W. Shan, J. Wu, A.M. Minor, *Nano Lett.* **11**(8), 3207 (2011)
48. M.A. Haque, H.D. Espinosa, H.J. Lee, *MRS Bull.* **35**(5), 375 (2010)
49. S. Bhowmick, H. Espinosa, K. Jungjohann, T. Pardoen, O. Pierron, *MRS Bull.* **44**(06), 487 (2019)
50. J. Rajagopalan, J.H. Han, M.T.A. Saif, *Science* **315**(5820), 1831 (2007)
51. L.Y. Chen, S. Terrab, K.F. Murphy, J.P. Sullivan, X. Cheng, D.S. Gianola, *Rev. Sci. Instrum.* **85**(1), 25 (2014)
52. U. Messerschmidt, F. Appel, *Ultramicroscopy* **1**(3–4), 223 (1976)
53. F. Mompiou, M. Legros, A. Sedlmayr, D.S. Gianola, D. Caillard, O. Kraft, *Acta Mater.* **60**(3), 977 (2012)
54. H. Zheng, A. Cao, C.R. Weinberger, J.Y. Huang, K. Du, J. Wang, Y. Ma, Y. Xia, S.X. Mao, *Nat. Commun.* **1**(9), 144 (2010)
55. A.M. Minor, S.A.S. Asif, Z.W. Shan, E.A. Stach, E. Cyrankowski, T.J. Wyrobek, O.L. Warren, *Nat. Mater.* **5**(9), 697 (2006)
56. Z.W. Shan, R.K. Mishra, S.A.S. Asif, O.L. Warren, A.M. Minor, *Nat. Mater.* **73**(7), 115 (2008)
57. C. Ophus, *Microsc. Microanal.* **25**(3), 563 (2019)
58. C. Gammer, J. Kacher, C. Czarnik, O.L. Warren, J. Ciston, A.M. Minor, *Appl. Phys. Lett.* **109**(8), 081906 (2016)
59. M.D. Demetriou, M.E. Launey, G. Garrett, J.P. Schramm, D.C. Hofmann, W.L. Johnson, R.O. Ritchie, *Nat. Mater.* **10**(2), 123 (2011)
60. M. Koyama, C.C. Tasan, E. Akiyama, K. Tsuzaki, D. Raabe, *Acta Mater.* **70**, 174 (2014)
61. A. Tatschl, O. Kolednik, *Mater. Sci. Eng. A* **339**(1–2), 265 (2003)
62. A.D. Kammers, S. Daly, *Exp. Mech.* **53**(9), 1743 (2013)
63. R. Rabe, J.M. Breguet, P. Schwaller, S. Stauss, F.J. Haug, J. Patscheider, J. Michler, *Thin Solid Films* **469–470**, 206 (2004)
64. D. Kiener, C. Motz, T. Schöberl, M. Jenko, G. Dehm, *Adv. Eng. Mater.* **8**(11), 1119 (2006)
65. M. Legros, D.S. Gianola, C. Motz, *MRS Bull.* **35**(5), 354 (2010)
66. R. Wheeler, P.A. Shade, M.D. Uchic, *J. Mater.* **64**(1), 58 (2012)
67. Y. Guo, J. Schwiedrzik, J. Michler, X. Maeder, *Acta Mater.* **120**, 292 (2016)
68. F. Wang, M.P. Echlin, A.A. Taylor, J. Shin, B. Bammes, B.D.A. Levin, M. De Graef, T.M. Pollock, D.S. Gianola, *Ultramicroscopy* **220**, 113160 (2021)
69. S. Korte, W.J. Clegg, *Scr. Mater.* **60**(9), 807 (2009)
70. C.A. Schuh, J.K. Mason, A.C. Lund, *Nature* **4**(8), 617 (2005)
71. B.N. Lucas, W.C. Oliver, *Metall. Mater. Trans. A Phys. Metall. Mater. Sci.* **30**(3), 601 (1999)

72. V. Maier, A. Leitner, R. Pippan, D. Kiener, *JOM* **67**(12), 2934 (2015)

73. J.M. Wheeler, J. Michler, *Rev. Sci. Instrum.* **84**(10), 101301 (2013)

74. J.C. Trenkle, C.E. Packard, C.A. Schuh, *Rev. Sci. Instrum.* **81**(7), 073901 (2010)

75. J.M. Wheeler, D.E.J. Armstrong, W. Heinz, R. Schwaiger, *Curr. Opin. Solid State Mater. Sci.* **19**(6), 354 (2015)

76. G. Tiphéne, P. Baral, S. Comby-Dassonneville, G. Guillonneau, G. Kermouche, J.-M. Bergheau, W. Oliver, J.-L. Loubet, *J. Mater. Res.* **36**(12), 2383 (2021)

77. C. Minnert, W.C. Oliver, K. Durst, *Mater. Des.* **192**, 108727 (2020)

78. A. Lupinacci, J. Kacher, A. Eilenberg, A.A. Shapiro, P. Hosemann, A.M. Minor, *Acta Mater.* **78**, 56 (2014)

79. S.-W. Lee, L. Meza, J.R. Greer, *Appl. Phys. Lett.* **103**(10), 101906 (2013)

80. J.M. Wheeler, J. Michler, *Rev. Sci. Instrum.* **84**(4), 045103 (2013)

81. J. Ast, J.J. Schwiedrzik, J. Wehrs, D. Frey, M.N. Polyakov, J. Michler, X. Maeder, *Mater. Des.* **152**, 168 (2018)

82. A. Leitner, V. Maier-Kiener, D. Kiener, *Mater. Res. Lett.* **5**(7), 486 (2017)

83. C. Minnert, K. Durst, *J. Mater. Res.* **37**(2), 567 (2021)

84. V. Maier-Kiener, K. Durst, *JOM* **69**(11), 2246 (1989)

85. V. Maier, K. Durst, J. Mueller, B. Backes, H.W. Höppel, M. Göken, *J. Mater. Res.* **26**(11), 1421 (2011)

86. J.M. Wheeler, V. Maier, K. Durst, M. Göken, J. Michler, *Mater. Sci. Eng. A* **585**, 108 (2013)

87. P. Sudharshan Phani, B.L. Hackett, C.C. Walker, W.C. Oliver, G.M. Pharr, *Curr. Opin. Solid State Mater. Sci.* **27**(1), 101054 (2023)

88. G. Guillonneau, M. Mieszala, J. Wehrs, J. Schwiedrzik, S. Grop, D. Frey, L. Philippe, J.-M. Breguet, J. Michler, J.M. Wheeler, *Mater. Des.* **148**, 39 (2018)

89. B.L. Hackett, P. Sudharshan Phani, C.C. Walker, W.C. Oliver, G.M. Pharr, *J. Mater. Res.* **38**(5), 1163 (2023)

90. B. Moser, K. Wasmer, L. Barbieri, J. Michler, *J. Mater. Res.* **22**(4), 1004 (2007)

91. T.E.J. Edwards, X. Maeder, J. Ast, L. Berger, J. Michler, *Sci. Adv.* **8**(30), eabo5735 (2022)

92. X. Ma, W. Higgins, Z. Liang, D. Zhao, G. Pharr, K. Xie, *Proc. Natl. Acad. Sci. U.S.A.* **118**, e2025657118 (2021)

93. G. Feng, W.D. Nix, *Scr. Mater.* **51**(6), 599 (2004)

94. L. Jiang, Z. Bai, M. Powers, Y. Fan, W. Zhang, E.P. George, A. Misra, *Mater. Sci. Eng. A* **848**, 143144 (2022)

95. J. Wang, A. Misra, *Curr. Opin. Solid State Mater. Sci.* **27**(1), 101056 (2023)

96. S.J. Wang, D.Y. Xie, J. Wang, A. Misra, *Mater. Sci. Eng. A* **800**, 140311 (2021)

97. B. Wei, W. Wu, D. Xie, H.-H. Lien, M. Kayitmazbatir, A. Misra, J. Wang, *Mater. Res. Lett.* **9**(12), 507 (2021)

98. H.-H. Lien, J. Wang, A. Misra, *Mater. Des.* **218**, 110701 (2022)

99. A. Chatterjee, E. Sprague, J. Mazumder, A. Misra, *Mater. Sci. Eng. A* **802**, 140659 (2021)

100. A. Misra, M. Göken, N.A. Mara, I.J. Beyerlein, *MRS Bull.* **46**(3), 236 (2021)

101. N. Mara, A. Sergueeva, A. Misra, A.K. Mukherjee, *Scr. Mater.* **50**(6), 803 (2004)

102. B.B. Zhang, Y.G. Tang, Q.S. Mei, X.Y. Li, K. Lu, *Science* **378**(6620), 659 (2022)

103. D. Kiener, A.M. Minor, O. Anderoglu, Y. Wang, S.A. Maloy, P. Hosemann, *J. Mater. Res.* **27**(21), 2724 (2012)

104. P. Hosemann, C. Shin, D. Kiener, *J. Mater. Res.* **30**(09), 1231 (2015)

105. N. Li, N.A. Mara, Y.Q. Wang, M. Nastasi, A. Misra, *Scr. Mater.* **64**(10), 974 (2011)

106. D. Kiener, P. Hosemann, S.A. Maloy, A.M. Minor, *Nat. Mater.* **10**, 608 (2011)

107. S.J. Dillon, D.C. Bufford, G.S. Jawaharram, X. Liu, C. Lear, K. Hattar, R.S. Averback, *J. Nucl. Mater.* **490**, 59 (2017)

108. H.J. Qu, K.H. Yano, P.V. Patki, M.J. Swenson, J.P. Wharry, *J. Mater. Res.* **35**(8), 1037 (2019)

109. M.J. Demkowicz, R.G. Hoagland, B.P. Uberuaga, A. Misra, *Phys. Rev. B* **84**(10), 104102 (2011)

110. Y. Yamamoto, B.A. Pint, K.A. Terrani, K.G. Field, Y. Yang, L.L. Snead, *J. Nucl. Mater.* **467**, 703 (2015)

111. Y. Cui, E. Aydogan, J.G. Gigax, Y. Wang, A. Misra, S.A. Maloy, N. Li, *Acta Mater.* **202**, 255 (2021)

112. V. Jayaram, *Annu. Rev. Mater. Res.* **52**(1), 473 (2022)

113. D. Kiener, S.M. Han, *MRS Bull.* **47**(8), 792 (2022)

114. S. Wurster, C. Motz, R. Pippan, *Philos. Mag.* **92**(14), 1803 (2012)

115. J. Kappacher, A. Leitner, D. Kiener, H. Clemens, V. Maier-Kiener, *Mater. Des.* **189**, 108499 (2020) ☐

Publisher's note

Daniel Kiener is professor of micro- and nanomechanics of materials in the Department of Materials Science at Montanuniversität Leoben, Austria. He received his PhD degree and habilitation in materials physics from Montanuniversität Leoben. His research focusses on linking mechanical properties of advanced materials to fundamental deformation and failure mechanisms to tailor their performance. His group develops and employs various scale-bridging testing schemes, with emphasis on miniaturized *in situ* experiments conducted in electron microscopes. Kiener can be reached by email at daniel.kiener@unileoben.ac.at.

Amit Misra is the Edward DeMille Campbell Collegiate Professor in the Department of Materials Science and Engineering at the University of Michigan, and director of the Michigan Materials Research Institute. From 1996 to 2014, he was employed at Los Alamos National Laboratory (LANL). His research group studies nanomechanics and metallic interfaces focusing on the design and development of multicomponent alloys, and multiphase materials for advanced structural applications. He is a Fellow of the Materials Research Society, The Minerals, Metals & Materials Society, AAAS, ASM International, and LANL. Misra can be reached by email at amitmis@umich.edu.